Tianbao Zheng*, Luca Azzolin, Jorge Sánchez, Olaf Dössel, and Axel Loewe

An automated pipeline for generating fiber orientation and region annotation in patient-specific atrial models

Abstract: Modeling the 'digital twin' of a patient's heart has gained traction in the last years and helps to understand the pathogenic mechanisms of cardiovascular disease to pave the way for personalized therapies. Although a 3D patient-specific model (PSM) can be obtained from computed tomography (CT) or magnetic resonance imaging (MRI), the fiber orientation of cardiac muscle, which significantly affects the electrophysiological and mechanical characteristics of the heart, can hardly be obtained in vivo. Several approaches have been suggested to solve this problem. However, most of them require a considerable amount of human interaction, which is both time-consuming and a potential source of error. In this work, a highly automated pipeline based on a Laplace-Dirichlet-rule-based method (LDRBM) for annotating fibers and anatomical regions in both atria is introduced. The calculated fiber arrangement was regionally compared with anatomical observations from literature and faithfully reproduced clinical and experimental data.

Keywords: patient-specific model, atrial modeling, atrial myofiber reconstruction, Laplace-Dirichlet-rule-based-method.

1 Introduction

Cardiovascular disease has been the world's leading cause of death for the past decades. Cardiac computational modelling and in-silico experiments have become essential in studying, diagnosing of cardiovascular disease, and personalizing patients' treatment. PSM can help to understand the pathological mechanisms of the heart and tailor therapy that

improves the patient's quality of life. However, building a digital twin of a patient's heart from clinical data from in vivo CT/MRI imaging or electro-anatomical maps without human interaction is not an easy task. Nowadays, techniques to reconstruct the 3D anatomy of the heart are available and, in some cases, partly automated. However, the myocardial fiber orientation and anatomical region annotation essential for creating a digital twin for electrophysiological simulations can hardly be reconstructed. In the atria, it is harder to reconstruct the fiber direction and annotate the anatomical regions than in the ventricles due to the thinner walls and more complex myocardial structures. Therefore, we aim to create an automated pipeline that reduces user interaction, robustly generates fiber fields and annotates the anatomical regions in the atrial independent from the geometry. Furthermore, the pipeline shall reduce the time needed to create the atrial digital twin.

2 Methods
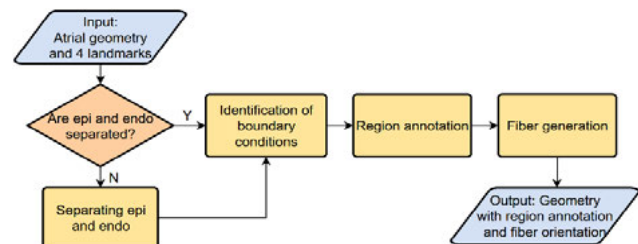
Figure 1: Flow chart of the pipeline where the input is an atrial geometry acquired from CT/MRI or electro-anatomical mapping.

The proposed pipeline, developed in python generates an atrial digital twin taking as input one 3D clinical acquired geometry such as from CT/MRI segmentation or from electro-anatomical maps (Figure 1). The only user interaction is picking four landmarks that are easy to identify on the atrial geometry, shown in Figure 3. Figure 1 shows the overall workflow of the pipeline. If the epicardium and endocardium of the geometry are distinguished, the pipeline will start annotating the regions and generating the fibers. Otherwise, the pipeline will firstly separate the epi- and endocardial surfaces.

———
* Corresponding author: Tianbao Zheng: Institute of Biomedical Engineering, Karlsruhe Institute of Technology (KIT), Kaiserstr. 12, 76131 Karlsruhe, Germany, E-mail: publications@ibt.kit.edu
Luca Azzolin, Jorge Sánchez, Olaf Dössel, Axel Loewe: Institute of Biomedical Engineering, Karlsruhe Institute of Technology (KIT), Kaiserstr. 12, 76131 Karlsruhe, Germany

2.1 Separating epi- and endocardial surfaces

To separate the epi- and endocardial surfaces, we propose a method inspired by the Poisson equation of electrostatics. Figure 2 shows the separation process. First, the local curvature of the model is calculated. Using a threshold and Density-Based Spatial Clustering of Applications with Noise (DBSCAN), the orifice rings of the atrium are identified. Using the center points of these orifices and the convex hull of the atrial model as boundary conditions, a Poisson problem is solved:

$$\nabla^2 u = f \tag{1}$$
$$u = 0 \qquad\qquad on\ \Gamma_a \tag{2}$$
$$\nabla u \cdot n = 0 \qquad\quad on\ \Gamma_n \tag{3}$$

The complete atrial surface and the convex hull are composing the "Faraday cage" Γ_a, where a zero Dirichlet boundary condition (Eq. 2) is imposed. The source term f consists of the "source charges" defined as the centers of the rings, where a value of one is applied. The Neumann boundary condition (Eq. 3) is applied to the rest region within the convex hull Γ_n. The result is an equipotential surface almost in contact with the endocardial surface of the atrium, as the dotted frame in Figure 2. The largest connected surface obtained when removing the closest points to the equipotential surface is the epicardium. Finally, the endocardial surface can be retrieved by taking the difference between the original closed surface and the epicardial surface.
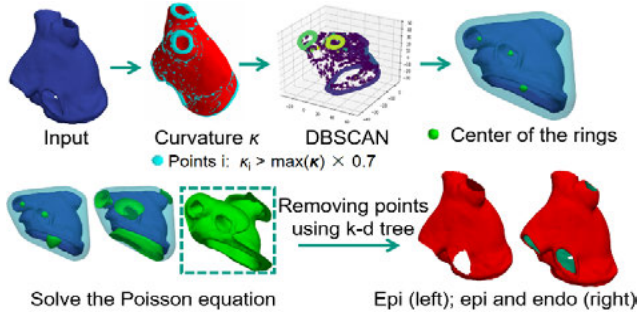
Figure 2: Separating the epi- and endocardial surfaces. The transparent light blue surface covering the atrium is the convex hull.

2.2 Identification of atrial feature areas

After separating the epi- and endocardial surfaces, the orifices of the atria (e.g., pulmonary veins, mitral valve) can be easily extracted from boundary edges. For the left atrium (LA), the largest ring was identified as the mitral valve (MV) Γ_{mv} and the rest of rings were clustered twice using k-means clustering in which the apex point of the left atrial appendage (LAA) Γ_{lap}

worked as a reference point. After the first clustering, the pulmonary veins were separated into left pulmonary veins (LPV) Γ_{lpv}, which are close to appendage, and right pulmonary veins (RPV) Γ_{rpv}. After the second clustering LPV and RPV were further separated into superior and inferior. Plane I and II in Figure 3 present schematically the hyperplanes of the first and the second k-means clustering. For the orifice rings of the right atrium (RA), the biggest one is identified as the tricuspid valve (TV) Γ_{tv}, the smallest one as coronary sinus (CS) Γ_{cs}, the one close to the apex point of the right atrial appendage (RAA) Γ_{rap} is the superior vena cava (SVC) Γ_{scv} and the remaining one the inferior vena cava (IVC) Γ_{icv}. Next, a plane passing through the centers of SVC, IVC and TV (plane III in Figure 3) divides the TV into two parts: septal (TV_S) Γ_{tv_s} and lateral (TV_W) Γ_{tv_w}. Finally, the line of intersection between this plane and the top of the right atrium is marked as Γ_{top}.
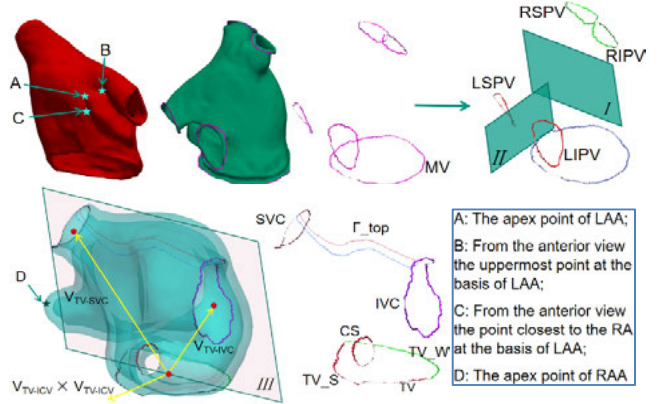
Figure 3: Landmarks and boundary conditions on the LA and the RA. The Landmarks A, B, C and D are marked with starts; I and II mark the schematic hyperplanes of k-means.

2.3 LDRBM

The Laplace equation was solved in openCARP [7] with Dirichlet boundary conditions to find a solution ψ. The value ψ_i and domain Γ_i of the boundary conditions for the nine Laplace equations are shown in Table 1. The results of the Laplace solutions are shown in Figure 4.
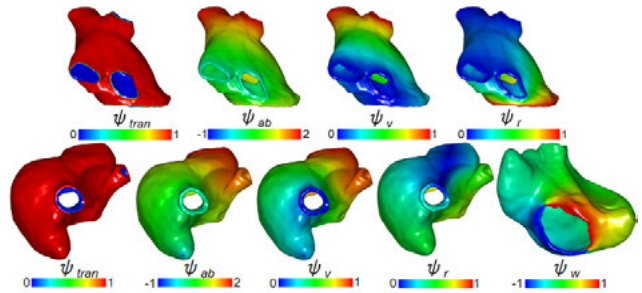
Figure 4: Visualized scalar field on the LA (top row) and the RA (bottom row) obtained by solving the Laplace problems defined in Table 1.

Table 1: Dirichlet and Neumann boundary conditions for 9 Laplace problems in the LA and the RA [2]

Type	ψ	ψ_a	Γ_a	ψ_b	Γ_b	Γ_n
	ψ_{tran}	1	Γ_{epi}	0	Γ_{endo}	
	ψ_{ab}	2	Γ_{rpv}	1	Γ_{mv}	Rest of regions
LA		0	Γ_{lpv}	-1	Γ_{lap}	
	ψ_v	1	Γ_{rpv}	0	Γ_{lpv}	
	ψ_r	1	Γ_{mv}	0	$\Gamma_{lpv} \cup \Gamma_{rpv} \cup \Gamma_{lap}$	
	ψ_{tran}	1	Γ_{epi}	0	Γ_{endo}	
	ψ_{ab}	2	Γ_{icv}	1	Γ_{tv}	Rest of regions
RA		0	Γ_{scv}	-1	Γ_{rap}	
	ψ_v	1	Γ_{icv}	0	$\Gamma_{scv} \cup \Gamma_{rap}$	
	ψ_r	1	Γ_{tv}	0	Γ_{top}	
	ψ_w	1	Γ_{tv_s}	-1	Γ_{tv_w}	

The Laplace solutions define a series of scalar fields ψ_i. By calculating the normalized gradients of ψ_i, we obtain the vector fields $\nabla\psi_i$. Based on the Laplace solutions, the bundle selection is carried out with a rule-based method. The principle was to apply thresholds on the Laplace solutions to intercept a certain region of the model and give the region a certain vector field and region tag. Based on the rules in [2], the left atrium (LA) bundle selection rule was modified and is presented in pseudo-code in Algorithm 1. For the RA, the process of distinguishing epi- and endocardial layers was added to the rules for the RA in [2], similar to (a) and (b) in Algorithm 1.

Algorithm 1 Bundle selection for LA

Every element of the geometry has attributes: R_1, R_2, ψ_i, $\nabla\psi_i$ and k; R_i is the region tag, k is the mapped gradient field on the geometry from $\nabla\psi_i$. $i \in \{tran, ab, v, r\}$

if $\psi_{tran} \geq 0.5$ **set** $R_1 \rightarrow epi$ (a)
else set $R_1 \rightarrow endo$ (b)
if $\psi_r \geq \tau_{mv}$ **set** $R_2 \rightarrow MV$, $k = \nabla\psi_r$
else
    if $\psi_v \geq \tau_{lpv}$ **set** $R_2 \rightarrow LPV$, $k = \nabla\psi_v$
    if $\psi_v \leq \tau_{rpv}$ **set** $R_2 \rightarrow RPV$, $k = \nabla\psi_v$
    else set $R_2 \rightarrow LAW$, $k = \nabla\psi_{ab}$
if $\psi_{tran} \geq 0.5$ **and** $\psi_r \geq \tau_{bb}$
    set $k = \nabla\psi_r$ **in** $posterior\ part\ of\ LA$ (c)

The values for τ_{mv}, τ_{tv}, τ_{icv}, τ_{scv}, τ_{ras}, τ_{raw} were 0.85, 0.9, 0.8, 0.2, 0.13, 0.55, respectively. τ_{lpv}, τ_{rpv}, τ_{bb}, and $\tau_{ct\text{-}}$ are geometry dependent. τ_{bb} is the value of ψ_r on the point B in Figure 3. τ_{lpv} and τ_{rpv} are determined by a region growing method. In the LA, the region is intercepted, where ψ_v is smaller than a dynamic threshold that decreasing from 1.

When the two pulmonary veins regions meet, the threshold at this moment is determined as τ_{rpv}, likewise for τ_{lpv}. For $\tau_{ct\text{-}}$, the inferior vena cava (IVC) and the superior vena cava (SVC) regions are first intercepted using the method from [2]. Next, the region on RA is intercepted, where ψ_w is smaller than a dynamic threshold that increasing from -1. When the region meets both IVC and SVC, $\tau_{ct\text{-}}$ is equal to the threshold.

After the bundle selection, at each element of the atrial domain, an orthonormal local coordinate system is built by performing a Gram–Schmidt orthogonalization process:

$$\hat{e}_n = \frac{k - (k \cdot \nabla\psi_{tran}) \cdot \nabla\psi_{tran}}{\|k - (k \cdot \nabla\psi_{tran}) \cdot \nabla\psi_{tran}\|} \tag{4}$$

$$\hat{e}_l = \hat{e}_n \times \nabla\psi_{tran} \tag{5}$$

The vector field $\hat{e}_l$ is the fiber orientation of the atrium. For the RA, an extra process is performed to annotate the crista terminalis (CT) and the pectinate muscles (PM). The region CT obtained from the rules in [2] was not accurate enough but faithfully identifies the start and end points of the CT. Two points close to the centers of mass of the intersecting areas between SVC/IVC and CT are selected as the start/end points. Between the start and end points, a geodesic path is created using Dijkstra's algorithm and smoothed by downsampling. The region around this path within 4.62 mm, based on the findings of [1], is tagged as CT with the fiber orientation following the geodesic path. 15 points uniformly distributed on CT and TV_S, corresponding in order in the direction from SVC to IVC, are used as the starting/ending points of the 15 PM [1]. Each point pair forms a plane with the center of the MV. The intersection area of this plane and the geometry is used as the search area. In the search area, a path is identified by Dijkstra's algorithm. The region around this path within 0.66 mm [1] is tagged as PM. The fiber orientation is parallel to the path. The result of annotating CT and PM is shown in Figure 5g. The LAA has a tubular and very patient-specific shape, which makes automatic identification of the LAA challenging. A plane passing through two automatically identified control points at the junctions of LPV and RPV and the center of mitral valve (MV) is used to divide the LA into anterior and posterior parts (Algorithm 1(c)). Four auxiliary points at the basis of the appendage are found automatically, which are similar to the points L5, L10, L34 and L12 in [1] by using the geodesic paths and smoothing. These points form a trajectory traveling around the basis of the appendage that isolates the appendage from the atrium. Using a rule-based method from [1] and the region tags obtained from the bundle selection, Bachmann's bundle, the middle posterior, the upper posterior and the coronary sinus bridges were merged using a boolean mesh operation.

3 Results
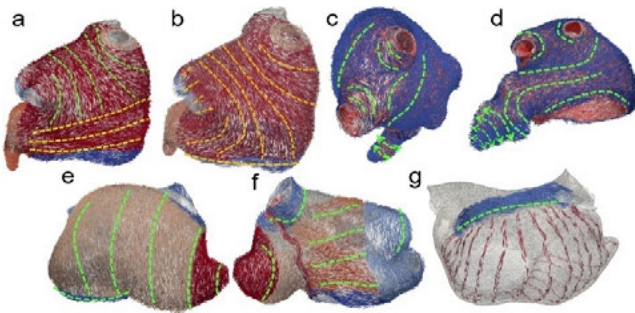
Figure 5: The generated fiber orientation of the LA (top row) and the RA (bottom row). The dashed lines show the main direction of fibers. a) epicardial layer, b) endocardial layer, c) + d) smooth transition at the junction of the LPV and the LAA, e) posterior view of RA, f) anterior view, g) CT and PM in the RA.

The generated fiber orientation and region annotations in the LA and RA are shown in Figure 5. The comparison with the anatomical observations of fiber orientation by Ho et al. [6] indicated a high degree of similarity. Furthermore, three different atrial geometries from [3], [4] and [5] were used to benchmark the pipeline. The results (Figure 6) show the robustness for different atrial geometries. For the meshes with an average edge length of 1.2-0.5 mm, the pipeline requires 6-30 minutes calculation time, respectively.
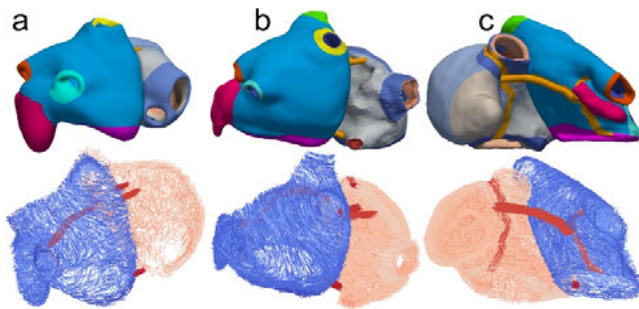
Figure 6: Three different atrial geometries from different sources: a [4], b [3] and c [5]. Top row: region annotation (color), bottom row: fiber orientation.

4 Discussion

We have developed a highly automated pipeline that accurately generates the fiber direction of the human atria according to histological data. Additionally, we provide an algorithm that annotates the anatomical regions independently from the atrial geometrical variability due to the region growing implementation. We demonstrate how the pipeline can augment 3D models with different average edge lengths,

copes with anatomical variations and creates accurate models of the human atrial anatomy. Comparing to the existing method from [1] that requires 21 manually defined seed points and a longer calculation time, our pipeline significantly reduces the calculating time and human manual interaction. In addition, to improve the automation of the pipeline, four seed points needed can be reduced by using an extra set of Laplace solutions. This Pipeline is based on the LDRBM proposed by Piersanti et al. [2], and the ideas of their method have inspired this work greatly.

Our novel pipeline for accurate annotation of fiber orientation and anatomical regions in the human atria accelerates the process of creating atrial digital twins and significantly reduces the required human interaction, thereby fostering the study of pathogenic mechanisms and tailored therapeutic approaches.

References

[1] Wachter A, Loewe A, Krueger M, et al., "Mesh structure-independent modeling of patient-specific atrial fiber orientation," Current Directions in Biomedical Engineering 1, 409–412, 2015.

[2] Piersanti R, Africa P, Fedele M, et al., "Modeling cardiac muscle fibers in ventricular and atrial electrophysiology simulations," vol. 373, Computer Methods in Applied Mechanics and Engineering, 2021, 113468.

[3] Roney CH, Bendikas R, Pashakhanloo F. et al., "Constructing a Human Atrial Fibre Atlas," Ann Biomed Eng 49, pp. 233–250, 2021.

[4] Nagel C, Schuler S, Dössel O, Loewe A, "A Bi-atrial Statistical Shape Model and 100 Volumetric Anatomical Models of the Atria," Zenodo, 2020. doi:10.5281/zenodo.4309958

[5] Loewe A, Krueger MW, Holmqvist F, Dössel O, Seemann G, and Platonov PG, "Influence of the earliest right atrial activation site and its proximity to interatrial connections on p-wave morphology," Europace, 18(suppl 4): iv35–iv43, 2016

[6] S. Y. Ho and D. Sanchez-Quintana, "The importance of atrial structure and fibers," Clinical Anatomy, vol. 22, no. 1, pp. 52–63, 1 2009.

[7] Plank G, Loewe A, Neic A, et al., "The openCARP Simulation Environment for Cardiac Electrophysiology." bioRxiv preprint, 2021. doi:10.1101/2021.03.01.433036